Anaplastic pleomorphic xanthoastrocytoma misdiagnosed as cerebral sparganosis—identification of the "mirror image"

Luji Liu, Lihong Zhang

Department of Neurology, The Second Hospital of Hebei Medical University, Shijiazhuang, China

Correspondence to: Lihong Zhang. Department of Neurology, The Second Hospital of Hebei Medical University, 215 Heping West Road, Shijiazhuang 050000, China. Email: lihongzhang_med@163.com.

Introduction

Anaplastic pleomorphic xanthoastrocytoma (aPXA) is a poorly differentiated pleomorphic xanthoastrocytoma, which has similar imaging features to cerebral sparganosis at a specific stage of the disease. However, aPXA is a rare and highly malignant astrocytoma. It is highly invasive, easily recurrent, and has a 5-year survival rate of no more than 57.1% (1). aPXA accounts for less than 0.5% of astrocytomas (2,3) and less than 0.05% of primary intracranial tumors (4). Only a very few aPXA cases have been reported since 1979 (5) to the best of our knowledge. Furthermore, aPXA is common in children and young adults and is rarely seen in patients over 40 years old (6). Our article reports a rare case of an elderly aPXA patient who was initially misdiagnosed with cerebral sparganosis and analyzes the cause of the misdiagnosis to increase awareness of aPXA among physicians.

Case presentation

All procedures performed in studies involving human participants were following the ethical standards of the institutional and/or national research committee(s) and with the Helsinki Declaration (as revised in 2013). Written informed consent was obtained from the patient.

A 69-year-old female was hospitalized due to intermittent seizures occurring over the previous 7 days. She presented with generalized tonic-clonic attacks accompanied by unconsciousness and urinary incontinence. The above symptoms appeared four times in total and lasted for 1 minute each time. She had no limb weakness or paresthesia, no nausea and vomiting, and no fever. Initial symptomatic treatment was given in a local hospital, and then the patient was transferred to our medical center. The patient denied a recent history of colds or diarrhea and had no history of hypertension, diabetes mellitus, coronary artery disease, alcohol, and substance abuse. Her blood pressure was 121/79 mmHg, and there was no fever on admission. Her neurological examination was as follows: she was conscious and spoke slowly; her bilateral pupillary reflexes were normal; no nasolabial sulci were shallow; extremity strength scores were level 5; the Babinski signs (−) in the bilateral, sensory, and ataxia fields were normal, and the meningeal irritation test was negative. Laboratory test results were as follows: routine blood, urine, and feces tests were normal; polymerase chain reaction tests for serum Epstein-Barr virus, cytomegalovirus, herpes simplex virus, and varicella-zoster virus were negative; anti-nuclear antibody and anti-phospholipid antibody tests were normal; and liver and kidney function, serum tumor biomarkers, thyroid function, and serum electrolytes were normal. Chest computerized tomography (CT) suggested mild interstitial changes in the lower lobes of the lung. The cerebrospinal fluid pressure was 190 mmH$_2$O, the protein was 0.17 g/L, and no white blood cells were found. Head magnetic resonance imaging (MRI) showed abnormal signals in the right frontal lobe, right frontal deep white matter, and genu of the corpus callosum, without obvious edema. Contrast-enhanced MRI (CE-MRI) displayed platy or multiple bead-like changes in the abnormal areas (*Figure 1*). According to the clinical presentation and imaging features, cerebral sparganosis could not be ruled out. We recommended
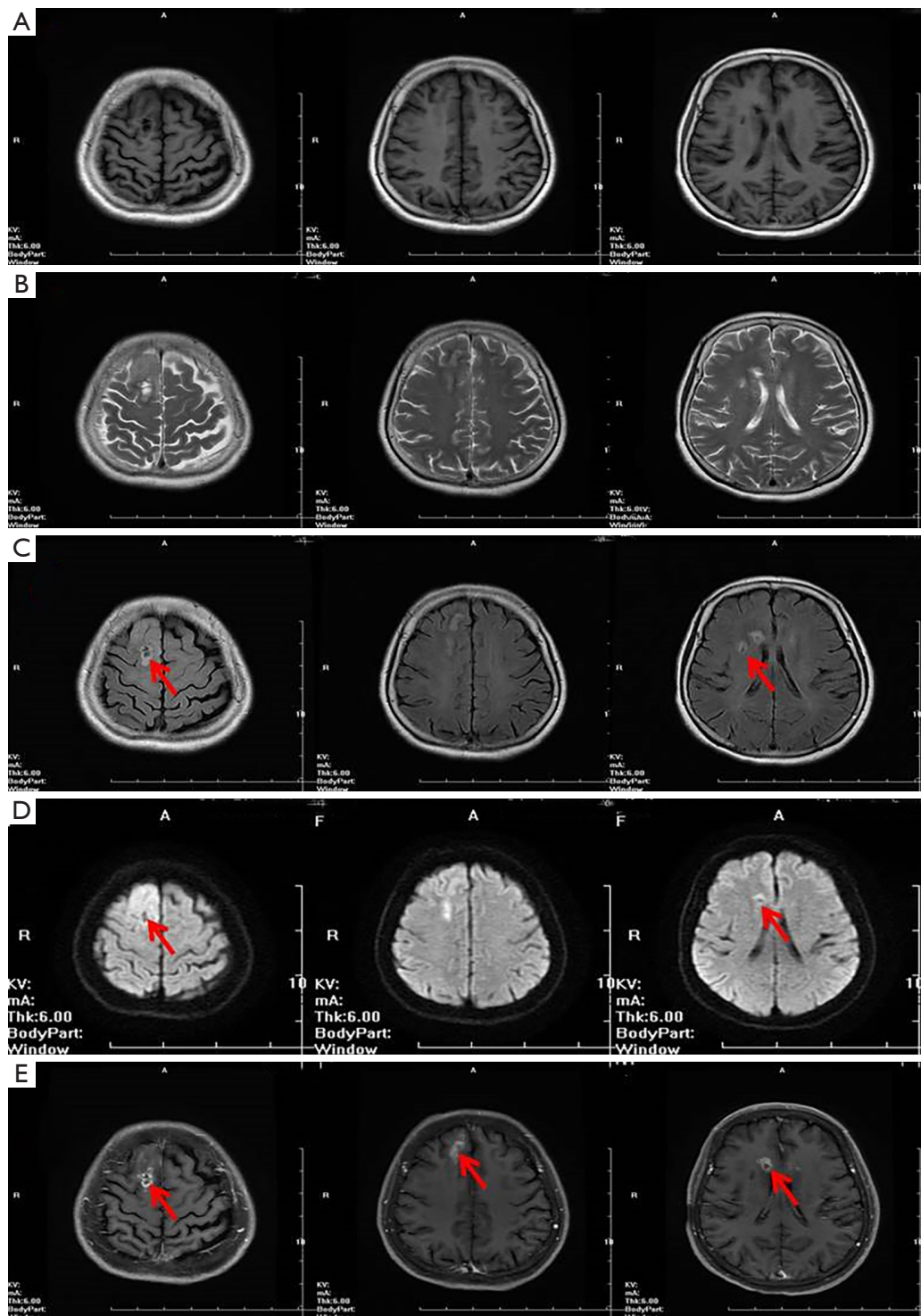
Figure 1 MRI of the first hospitalization; the lesions involve the right frontal lobe, right frontal deep white matter, and genu of the corpus callosum. (A) Lesions on T1WI show iso- or hypo-signal; (B) lesions on T2WI show iso- or hyper-signal; (C,D) lesions on FLAIR and DWI show hyper-signal, the right frontal lobe has cystic changes (arrow); (E) enhanced scanning shows patchy or multiple beaded signals (arrow). MRI, magnetic resonance imaging; T1WI, T1-weighted image; T2WI, T2-weighted image; FLAIR, fluid-attenuated inversion recovery; DWI, diffusion-weighted imaging.

the patient receive a parasite antibody examination, but she refused our suggestion and was discharged. Two months later, the patient reported left limb weakness, which had been gradually worsening. The neurological examination revealed dysarthria, asymmetric nasolabial sulci, level 4 left limb strength, and positive Babinski signs on the left side. Head MRI revealed that the lesion scope of the right frontal lobe and corpus callosum was significantly enlarged, and edema was obvious around the lesions (*Figure 2*). Magnetic Resonance Spectrum (MRS) suggested that the lipid (Lip) peak at the cystic lesion was increased, and the choline (Cho) peak was also increased at the solid lesion. However, the N-acetylaspartic acid (NAA) peak was decreased, which indicated that cell division was active (*Figure 3*). These findings suggested the possibility of a malignant tumor, so surgical resection was performed. The lesion tissue was fixed in 10% neutral formaldehyde solution, dehydrated, embedded in paraffin, and sectioned continuously. Hematoxylin-exosin and immunohistochemical staining were subsequently performed. Pathological examination revealed that the cells were pleomorphic, with monocytes, spindle cells, fat-rich foam cells, and local lymphocyte infiltration. Furthermore, there was marked mitosis (>5/HFP) and local necrosis. Immunohistochemical staining revealed GFAP (+), CD34 (+), Ki-67 (+15%), and S-100 (+) (*Figure 4*). Genetic tests revealed that there was no mutation in BRAFV600E. Given all of the above, the patient was diagnosed with aPXA and unfortunately died of respiratory and circulatory failure 5 months later.

Discussion

The clinical manifestations of aPXA are nonspecific, and seizure is the most common symptom (7). The temporal lobe is the most common distribution site of aPXA (8), followed by the parietal, occipital, and frontal lobes. Cases involving the cerebellum, ventricle, thalamus, spinal cord, pineal gland, and retina have also been reported (9) as submeningeal astrocytes form aPXA with lesions mainly distributed in the cerebral cortex (5). In our case, the lesions were found in the frontal cortex, subcortical white matter, and corpus callosum. Although these are not the most common sites of the disease, they have been reported in previous literature. In addition, the patient's symptoms were nonspecific. Therefore, clinical symptoms and sites of involvement were not able to help us make a definite diagnosis. Although aPXA is more common in young

people, it cannot be ruled out in older people, as in our case.

In MRI, aPXA usually shows as a solid mass or cystic mass with mural nodules located in the cerebral cortex. Due to the aggressive growth of the tumor cells, necrosis and cystic changes are easily seen in the focus area (10). In CE-MRI, aPXA is divided into three types: solid, cystic, and cystic-solid, with the cystic-solid type being the most common. The cystic-solid type can be further classified as large cystic with a mural nodule enhancement type and mass enhancement with a few cystic changes (11). In addition, in some patients, the lesions involve leptomeninges, while the endocranium is not generally involved (12). There is obvious edema around the tumor, and in some critical patients, the midline may shift (13). On MRI, the solid part of the lesion shows iso- or hypo-signal on T1-weighted imaging (T1WI) and iso- or hyper-signal on T2-weighted imaging (T2WI) (14), and the lesions are mostly supratentorial (15), which are similar to other intracranial tumors. MRS shows that the Cho peak and choline/creatinine (Cho/Cr) are increased, the NAA peak is decreased, and the Cho/NAA is increased in the diseased regions, indicating that the malignant tumors originate from astrocytes. The focus also shows restricted diffusion (16), which is closely related to the increased water molecules in the nucleus of the tumor cells. Perfusion-weighted imaging (PWI) shows an increased blood flow volume, which suggests microvascular hyperplasia in the anaplastic cells and an abundant blood flow in aPXA (17,18). Because aPXA is highly malignant, its volume can increase significantly in a short time, and the recurrence interval of aPXA after total surgical resection is 14 months (19). In our case, necrosis, cystic degeneration, and peripheral edema were not observed in the initial lesions, so it was difficult to diagnose malignant tumors. Therefore, we suggest that MRI examination alone is not conducive to a definite diagnosis in the early stage of aPXA due to the lack of characteristic imaging findings.

The diagnosis of aPXA is mainly based on pathological features, including cell pleomorphism (5), cell mitosis ≥5/high power field (HPF) (20), local lymphocyte infiltration, and local tissue necrosis (7,21). However, histopathology alone does not entirely rule out other diseases and needs to be combined with other indicators, such as cytokines, immunohistochemistry, gene mutations, and spectral analysis. Immunohistochemical staining of this case revealed GFAP (+), which indicated that the tumor tissue was derived from astrocytes (22). Moreover, 84% of patients demonstrate CD34 (+), and 17% have BRAFV600E
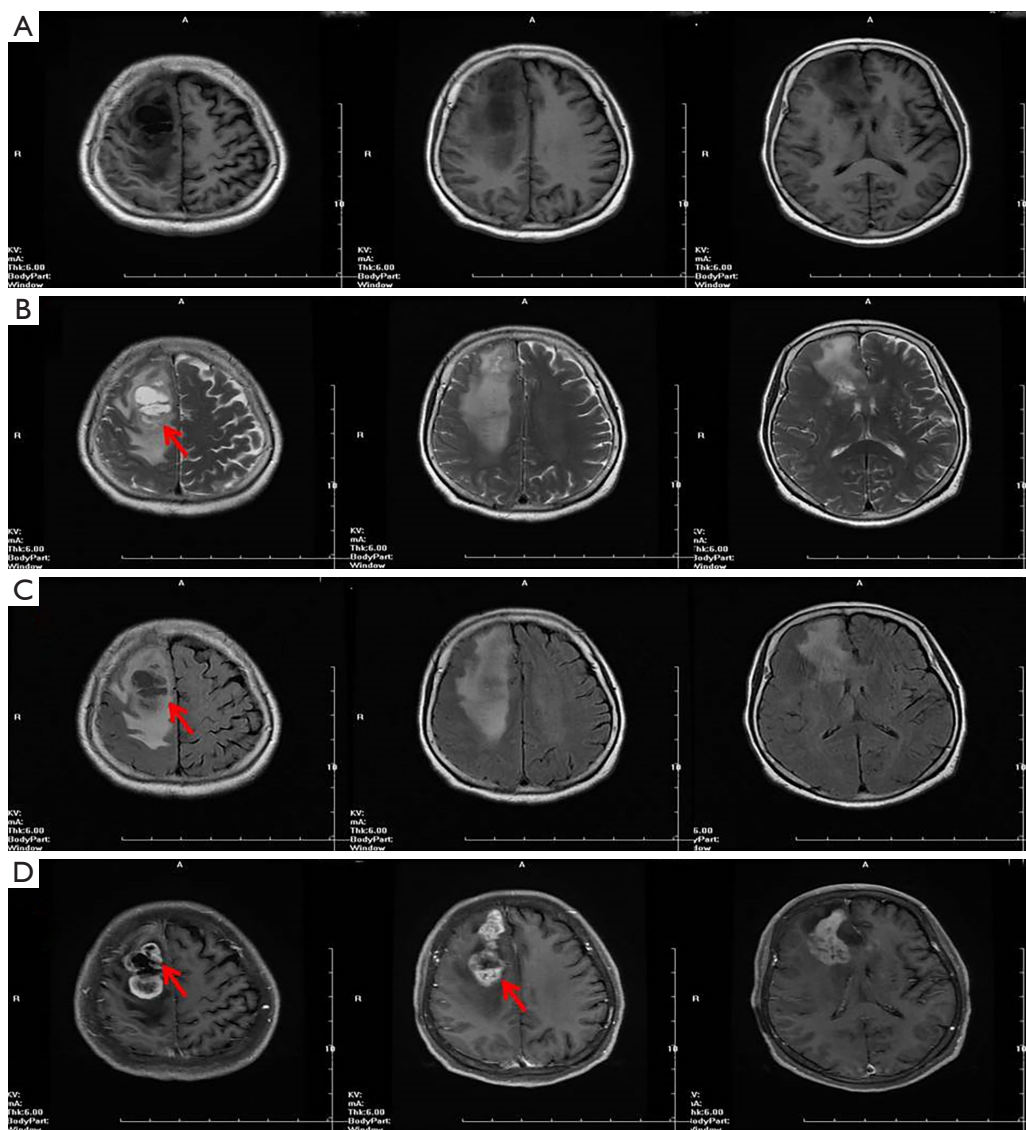
Figure 2 MRI shows that the lesions and edema are more evident after 2 months. (A) Lesions on T1WI shows hypo-signal; (B) lesions on T2WI shows hyper-signal and multiple cystic changes in lesions (arrow); (C) hyper-signal with multiple cystic changes in FLAIR (arrow); (D) enhanced scanning shows nodular or ring-like lesions, and a solid enhancement at the edge of the ring-like lesions (arrow). MRI, magnetic resonance imaging; T1WI, T1-weighted image; T2WI, T2-weighted image; FLAIR, fluid-attenuated inversion recovery.

mutations. In MRS, an increased Cho suggested glial cell proliferation, while a decreased NAA suggested neuron injury. All of the above results in our case supported the diagnosis of aPXA.

Sparganosis mansoni is caused by the larvae of the spirometra mansoni parasite in the human body. In China, sparganosis mansoni invades the central nervous system in approximately one out of every eight cases, and most cases are due to drinking contaminated water or eating uncooked

frogs, snakes, or other animals (23,24). Cerebral sparganosis can occur at any age, and its clinical presentations are diverse, including seizures, limb weakness, and coma (23).

CT shows hypo-density lesions in patients with cerebral sparganosis. MRI displays a hypo-signal on T1WI and a hyper-signal on T2WI without specificity (25). CE-MRI reveals a specific bead-like enhancement, known as the "nodule sign" (26). In addition, tubular signs can also be seen on MRI. In fluid-attenuated inversion recovery
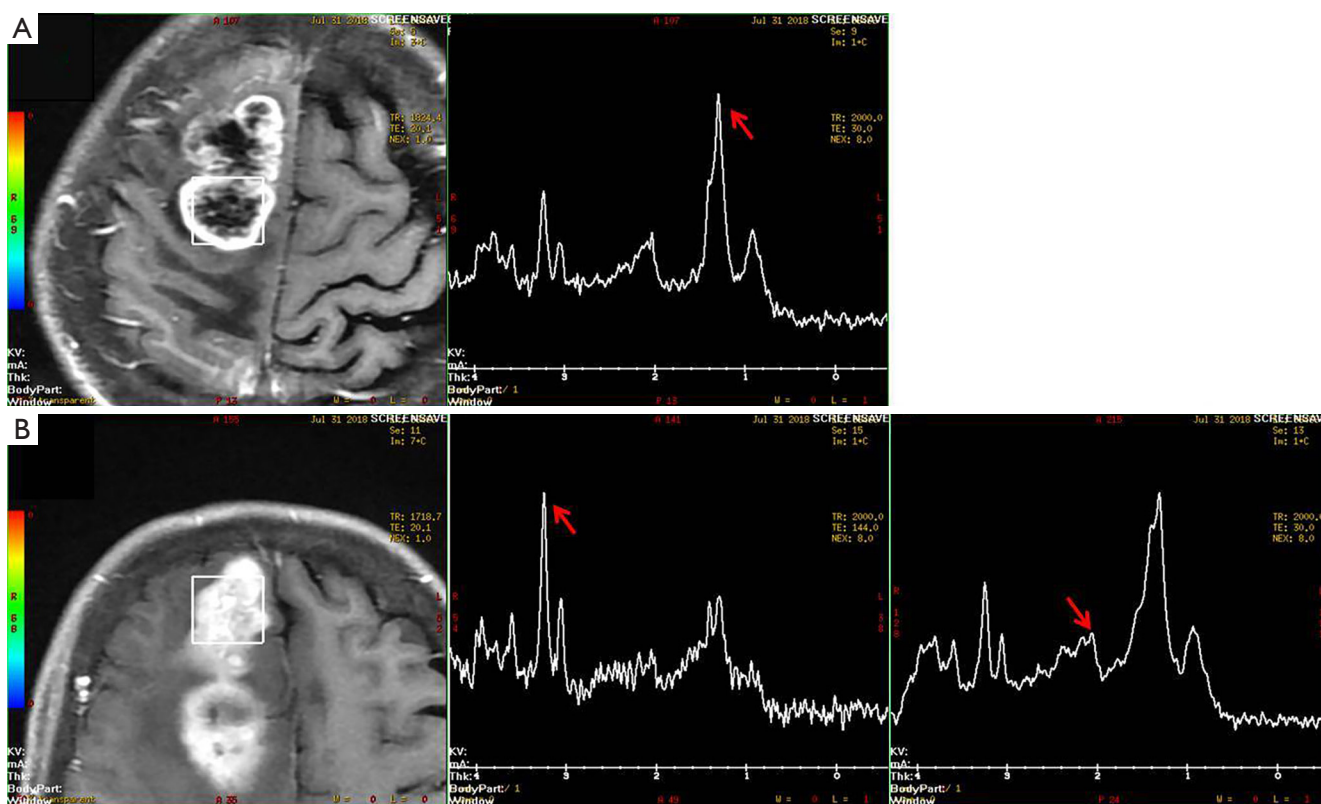
Figure 3 MRS imaging. (A) Lip peak is increased at cystic lesions (arrow); (B) cho peak is increased, and NAA peak is decreased in solid lesions (arrow). MRS, magnetic resonance spectrum; Lip, lactic acid; Cho, choline; NAA, N-acetyl aspartic acid.

(FLAIR), some lesions present as two bands of hyper-signal edema and one band of hypo-signal, or an equal-signal shadow between them, suggesting orbital-like changes. In CE-MRI, the orbital-like changes may have an enhanced appearance called the "tunnel sign" (27). It represents the track of the worm activity, but the worm activity is very slow and requires more than one check to detect this phenomenon.

Moreover, some lesions have "comma-like" enhancement. The coexistence of old and new lesions in the intracranial region is also characteristic of images found in cerebral sparganosis. In addition, there are various cystic changes in cerebral sparganosis, and CE-MRI reveals an enhanced cystic wall that is easily confused with cystic type aPXA. MRS shows the Cho peak increases, and the NAA peak is decreased, which is similar to aPXA. However, the lesions show hypoperfusion, which differs from glioma (28). Diffusion-weighted imaging (DWI) shows hyper-signal or hypo-signal, which is related to the survival state of the worm (29).

In some cases, ipsilateral ventricular dilatation, focal cortical atrophy, calcification, and white matter edema were observed (30). A small number of patients with cerebral sparganosis are difficult to diagnose by imaging alone but can be diagnosed by pathology. The characteristic pathology manifestations are "sinus tract", owing to local brain degeneration or necrosis (31).

In our case, the seizure was the initial main symptom, and MRI showed a progression from one frontal lobe to the contralateral side through the deep white matter, similar to the atypical "tunnel sign" in cerebral sparganosis. Additionally, the CE-MRI showed a bead-like lesion in our patient when first hospitalized, similar to the "nodal sign" of cerebral sparganosis. Furthermore, the incidence of aPXA in the elderly is rare, and involvement of the deep white matter and the corpus callosum are unusual. Therefore, during the first hospitalization, a diagnosis of cerebral sparganosis was proposed. However, unlike cerebral sparganosis, the clinical symptoms and imaging features progressed rapidly in a short time. Simultaneously, MRS supported a malignant lesion, and aPXA was finally confirmed by histopathology, immunohistochemistry, and
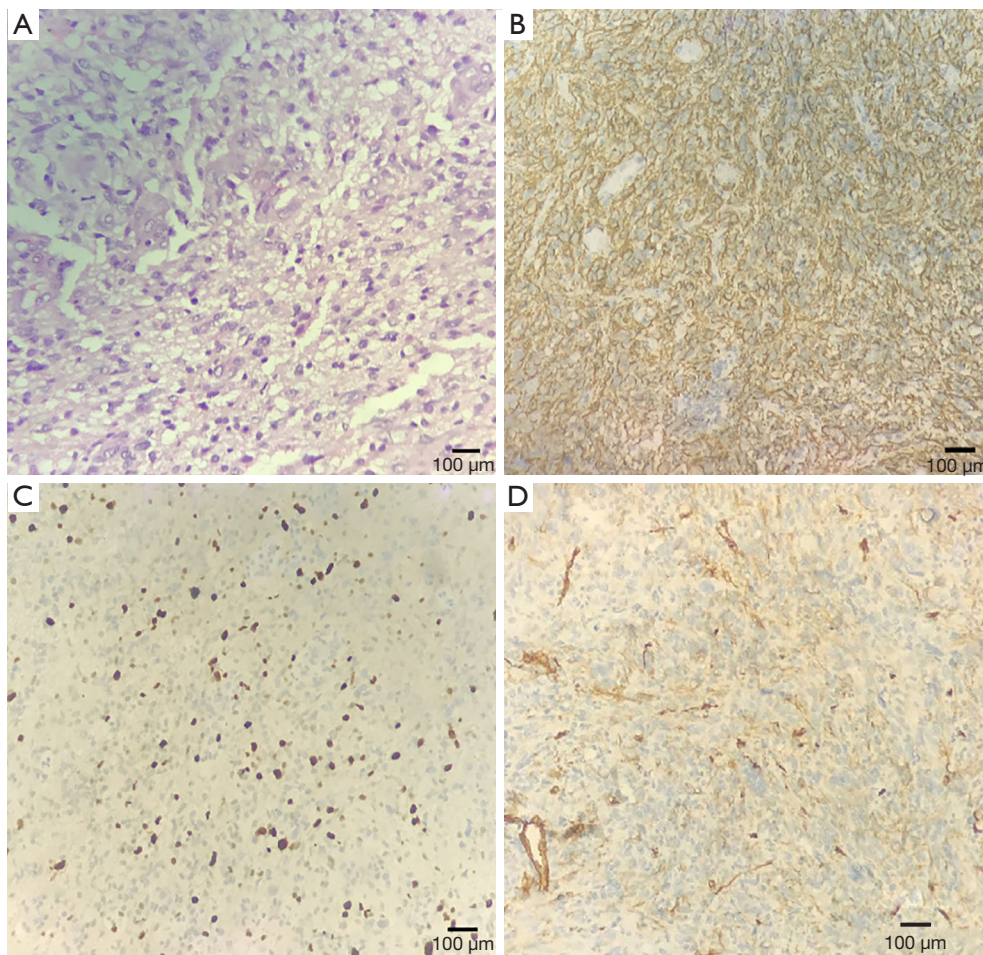
Figure 4 Microphotographs of the tumor with hematoxylin-eosin (HE) and immunohistochemical staining. (A) HE staining (×40) shows highly pleomorphic cell populations, with some demonstrating hyalinization and necrosis. (B) The tumor cells are immunopositive for GFAP (+). C:Ki-67 (+). D: CD34 (+). GFAP, glial fibrillary acidic protein.

gene testing.

Although most similar to sparganosis mansoni, our patient still required a differential diagnosis from other diseases. Primary central nervous system lymphoma (PCNSL) is a rare but aggressive form of extranodal non-Hodgkin lymphoma limited to the brain. The involvement of the corpus callosum and extension to the contralateral side of the brain can mimic glioblastoma multiforme (32,33). One of the histopathologic features of PCNSL is high cellularity with tightly compacted cells and a high nuclear to cytoplasmic ratio, which translates into some important image characteristics of PCNSL, such as iso- or hyperdense lesions in unenhanced CT, hyperintensity on DWI, and hypointensity on the apparent deficient coefficient (ADC) (34). The characteristic appearance of PCNSL on

MRI is of iso- to hypointensity on T1WI and hypointensity on T2WI. A gadolinium contrast MRI is the most sensitive imaging modality in the diagnosis of PCNSL. It is characterized by homogenous contrast enhancement with well-defined borders (35), which is different from aPXA. On MRS, the most common features of PCNSL include extremely high levels of lipids, which have also been used to distinguish glioblastoma multiforme (32). In addition, we needed to rule out central nervous system vasculitis. Primary angiitis of the central nervous system (PACNS) has a very similar MRI profile to our patient. The MRI features of PACNS are extremely variable and may mimic demyelinating diseases, infarction, cerebral parasitic diseases, and tumor-like lesions, such as glioma or lymphoma. It is mainly observed in unilateral supratentorial

lesions, with the frontal lobe as the center.

Nevertheless, deep white matter, like the corpus callosum, is also involved (36). The characteristics of focus enhancement are more common in unilateral supratentorial cerebral hemispherical mass enhancement, which can be reinforced with banded and linear and is partly accompanied by edema and an occupying effect. A midline displacement is also visible (37). DWI usually presents with a hyper-signal, and the ADC has a hypo-signal. PWI of PACNS shows hypo-perfusion, while the PWI of gliomas shows hyper-perfusion. Therefore, PWI is a valuable tool for identifying lesions, such as PACNS and other brain tumors (38).

Furthermore, as the blood vessels of PACNS patients were liable to rupture and hemorrhage, susceptibility-weighted imaging (SWI) would be helpful for diagnosis and differential diagnosis (39). Of note, glioblastoma and aPXA have very similar imaging and histopathology features and are very susceptible to misdiagnosis. Therefore, it is important to discriminate between the two diseases using other biomarkers and even molecular diagnostics. For example, the lesions of glioblastoma spread into the brain white matter and often invade the contralateral side through the corpus callosum, which is very similar to the image findings in our case. However, glioblastomas rarely express CD34 and BRAF mutations.

Conclusions

aPXA is an unusual and highly malignant astrocytoma and completely different from cerebral sparganosis in etiology, pathogenesis, pathology, and prognosis. However, the clinical manifestations and imaging findings of the two diseases are similar at a specific stage, which may easily cause misdiagnosis. Therefore, clinicians need to make a comprehensive judgment based on historical epidemiology, clinical manifestations, parasite antibody tests, and imaging findings. The pathological results are the "gold standard" for diagnosis.

Acknowledgments

Footnote

Conflicts of Interest: Both authors have completed the ICMJE uniform disclosure form (available at http://dx.doi.org/10.21037/qims-20-1398). The authors have no conflicts of interest to declare.

Ethical Statement: The authors are accountable for all aspects of the work in ensuring that questions related to the accuracy or integrity of any part of the work are appropriately investigated and resolved. All procedures performed in studies involving human participants were in accordance with the ethical standards of the institutional and/or national research committee(s) and with the Helsinki Declaration (as revised in 2013). Written informed consent was obtained from the patient.

References

1. Rutkowski MJ, Oh T, Niflioglu GG, Safaee M, Tihan T, Parsa AT. Pleomorphic Xanthoastrocytoma with Anaplastic Features: Retrospective Case Series. World Neurosurg 2016;95:368-74.
2. Hirose T, Ishizawa K, Sugiyama K, Kageji T, Ueki K, Kannuki S. Pleomorphic xanthoastrocytoma: a comparative pathological study between conventional and anaplastic types. Histopathology 2008;52:183-93.
3. Rao AA, Laack NN, Giannini C, Wetmore C. Pleomorphic xanthoastrocytoma in children and adolescents. Pediatr Blood Cancer 2010;55:290-4.
4. Ida CM, Rodriguez FJ, Burger PC. Pleomorphic Xanthoastrocytoma: Natural History and Long-Term Follow-Up. Brain Pathol 2015;25:575-86.
5. Choudry UK, Khan SA, Qureshi A, Bari E. Primary anaplastic pleomorphic xanthoastrocytoma in adults. Case report and review of literature. Int J Surg Case Rep 2016;27:183-8.
6. Marton E, Feletti A, Orvieto E, Longatti P. Malignant progression in pleomorphic xanthoastrocytoma: personal experience and review of the literature. J Neurol Sci 2007;252:144-53.

7. Patibandla MR, Nayak M, Purohit AK, Thotakura AK, Uppin M, Challa S. Pleomorphic xanthoastrocytoma with anaplastic features: A rare case report and review of literature with reference to current management. Asian J Neurosurg 2016;11:319.

8. Yu S, He L, Zhuang X, Luo B. Pleomorphic xanthoastrocytoma: MR imaging findings in 19 patients. Acta Radiol 2011;52:223-8.

9. Hamlat A, Le Strat A, Guegan Y, Ben-Hassel M, Saikali S. Cerebellar pleomorphic xanthoastrocytoma: case report and literature review. Surg Neurol 2007;68:89-94; discussion 94-5.

10. Crespo-Rodríguez AM, Smirniotopoulos JG, Rushing EJ. MR and CT imaging of 24 pleomorphic xanthoastrocytomas (PXA) and a review of the literature. Neuroradiology 2007;49:307-15.

11. Yeh DJ, Hessler RB, Stevens EA, Lee MR. Composite pleomorphic xanthoastrocytoma-ganglioglioma presenting as a suprasellar mass: case report. Neurosurgery 2003;52:1465-8; discussion 1468-9.

12. Iwaki T, Fukui M, Kondo A, Matsushima T, Takeshita I. Epithelial properties of pleomorphic xanthoastrocytomas determined in ultrastructural and immunohistochemical studies. Acta Neuropathol 1987;74:142-50.

13. Lim S, Kim JH, Kim SA, Park ES, Ra YS, Kim CJ. Prognostic factors and therapeutic outcomes in 22 patients with pleomorphic xanthoastrocytoma. J Korean Neurosurg Soc 2013;53:281-7.

14. Gonçalves VT, Reis F, Queiroz Lde S, França M Jr. Pleomorphic xanthoastrocytoma: magnetic resonance imaging findings in a series of cases with histopathological confirmation. Arq Neuropsiquiatr 2013;71:35-9.

15. Gallo P, Cecchi PC, Locatelli F. Pleomorphic xanthoastrocytoma: long-term results of surgical treatment and analysis of prognostic factors. Br J Neurosurg 2013;27:759-64.

16. Moore W, Mathis D, Gargan L. Pleomorphic xanthoastrocytoma of childhood: MR imaging and diffusion MR imaging features. AJNR Am J Neuroradiol 2014;35:2192-6.

17. She D, Liu J, Xing Z, Zhang Y, Cao D, Zhang Z. MR Imaging Features of Anaplastic Pleomorphic Xanthoastrocytoma Mimicking High-Grade Astrocytoma. AJNR Am J Neuroradiol 2018;39:1446-52.

18. Goyal P, Kumar Y, Gupta N, Malhotra A, Gupta S, Gupta S, Mangla M, Mangla R. Usefulness of enhancement-perfusion mismatch in differentiation of CNS lymphomas from other enhancing malignant tumors of the brain.

Quant Imaging Med Surg 2017;7:511-9.

19. Kim B, Chung CK, Myung JK, Park SH. Pleomorphic xanthoastrocytoma associated with long-standing Taylor-type IIB-focal cortical dysplasia in an adult. Pathol Res Pract 2009;205:113-7.

20. Shaikh N, Brahmbhatt N, Kruser TJ. Pleomorphic xanthoastrocytoma: a brief review. CNS Oncol 2019;8:CNS39.

21. Tonse R, Gupta T, Epari S. Impact of WHO 2016 update of brain tumor classification, molecular markers and clinical outcomes in pleomorphic xanthoastrocytoma. J Neurooncol 2018;136:343-50.

22. Tonn JC, Paulus W, Warmuth-Metz M, Schachenmayr W, Sörensen N, Roosen K. Pleomorphic xanthoastrocytoma: report of six cases with special consideration of diagnostic and therapeutic pitfalls. Surg Neurol 1997;47:162-9.

23. Gong C, Liao W, Chineah A, Wang X, Hou BL. Cerebral sparganosis in children: epidemiological, clinical and MR imaging characteristics. BMC Pediatr 2012;12:155.

24. Xie D, Wang M, Chen X, Tuo HZ. A case report: 1-year follow-up of cerebral sparganosis mansoni with a stroke-like onset. BMC Neurol 2019;19:105.

25. Adler BL, Kim GH, Kim DD. Image Gallery: Cerebral and subcutaneous sparganosis. Br J Dermatol 2020;182:e158.

26. Song T, Wang WS, Zhou BR. CT and MR characteristics of cerebral sparganosis. AJNR Am J Neuroradiol 2007;28:1700-5.

27. Peh WM, Hean GG, Clement Y. The Tunnel Sign Revisited: A Novel Observation of Cerebral Melioidosis Mimicking Sparganosis. J Radiol Case Rep 2018;12:1-11.

28. Chiu CH, Chiou TL, Hsu YH, Yen PS. MR spectroscopy and MR perfusion character of cerebral sparganosis: a case report. Br J Radiol 2010;83:e31-4.

29. Li YX, Ramsahye H, Yin B, Zhang J, Geng DY, Zee CS. Migration: a notable feature of cerebral sparganosis on follow-up MR imaging. AJNR Am J Neuroradiol 2013;34:327-33.

30. Yu Y, Shen J, Yuan Z. Cerebral Sparganosis in Children: Epidemiologic and Radiologic Characteristics and Treatment Outcomes: A Report of 9 Cases. World Neurosurg 2016;89:153-8.

31. Lo Presti A, Aguirre DT, De Andrés P, Daoud L, Fortes J, Muñiz J. Cerebral sparganosis: case report and review of the European cases. Acta Neurochir (Wien) 2015;157:1339-43; discussion 1343.

32. Löw S, Han CH, Batchelor TT. Primary central nervous system lymphoma. Ther Adv Neurol Disord

2018;11:1756286418793562.

33. Malikova H. Primary central nervous system lymphoma: is whole-body CT and FDG PET/CT for initial imaging reasonable. Quant Imaging Med Surg 2019;9:1615-8.

34. Chukwueke UN, Nayak L. Central Nervous System Lymphoma. Hematol Oncol Clin North Am 2019;33:597-611.

35. Nabavizadeh SA, Vossough A, Hajmomenian M, Assadsangabi R, Mohan S. Neuroimaging in Central Nervous System Lymphoma. Hematol Oncol Clin North Am 2016;30:799-821.

36. Huang YJ, Zhang L, Mao Y, Nan GX. Ataxia as the main manifestation of tumor-like primary angiitis of the central nervous system: a case report and literature review. BMC Med Imaging 2019;19:79.

37. Lee JS, Jung TY, Lee KH, Kim SK. Primary Central Nervous System Vasculitis Mimicking a Cortical Brain Tumor: A Case Report. Brain Tumor Res Treat 2017;5:30-3.

38. Lee Y, Kim JH, Kim E, Park SH, Yim YJ, Sohn CH. Tumor-mimicking primary angiitis of the central nervous system: initial and follow-up MR features. Neuroradiology 2009;51:651-9.

39. Sun LI, Zhu L, Zhao T, Wang D, Ma D, Zhang R. A rare case of tumor-mimicking primary angiitis of the central nervous system. Mol Clin Oncol 2016;4:827-29.